



**HAL**  
open science

## Degassing and gas percolation in basaltic magmas

Mathieu Colombier, Jeremie Vasseur, Bruce F. Houghton, Francisco Cáceres, Bettina Scheu, Ulrich Kueppers, Simon Thivet, Lucia Gurioli, Cristian Montanaro, Arianna Soldati, et al.

► **To cite this version:**

Mathieu Colombier, Jeremie Vasseur, Bruce F. Houghton, Francisco Cáceres, Bettina Scheu, et al.. Degassing and gas percolation in basaltic magmas. *Earth and Planetary Science Letters*, 2021, 573, 10.1016/j.epsl.2021.117134 . insu-03589884

**HAL Id: insu-03589884**

**<https://insu.hal.science/insu-03589884>**

Submitted on 28 Feb 2022

**HAL** is a multi-disciplinary open access archive for the deposit and dissemination of scientific research documents, whether they are published or not. The documents may come from teaching and research institutions in France or abroad, or from public or private research centers.

L'archive ouverte pluridisciplinaire **HAL**, est destinée au dépôt et à la diffusion de documents scientifiques de niveau recherche, publiés ou non, émanant des établissements d'enseignement et de recherche français ou étrangers, des laboratoires publics ou privés.



Distributed under a Creative Commons Attribution - NoDerivatives 4.0 International License



## Degassing and gas percolation in basaltic magmas

Mathieu Colombier<sup>a,\*</sup>, Jeremie Vasseur<sup>a</sup>, Bruce F. Houghton<sup>b</sup>, Francisco Cáceres<sup>a</sup>, Bettina Scheu<sup>a</sup>, Ulrich Kueppers<sup>a</sup>, Simon Thivet<sup>a,c</sup>, Lucia Gurioli<sup>c</sup>, Cristian Montanaro<sup>a</sup>, Arianna Soldati<sup>a,d</sup>, Andrea Di Muro<sup>e,f</sup>, Donald B. Dingwell<sup>a</sup>

<sup>a</sup> Department of Earth and Environmental Sciences, Ludwig-Maximilians-Universität, München, Germany

<sup>b</sup> Department of Earth Sciences, University of Hawai'i at Mānoa, Honolulu, HI 96822, USA

<sup>c</sup> Université Clermont Auvergne, CNRS, IRD, OPGC, Laboratoire Magmas et Volcans, F-63000 Clermont-Ferrand, France

<sup>d</sup> Department of Marine, Earth, and Atmospheric Sciences, North Carolina State University, USA

<sup>e</sup> Université de Paris, Institut de physique du globe de Paris, CNRS, F-75005 Paris, France

<sup>f</sup> Observatoire volcanologique du Piton de la Fournaise, Institut de physique du globe de Paris, F-97418 La Plaine des Cafres, France

### ARTICLE INFO

#### Article history:

Received 7 May 2021

Received in revised form 23 July 2021

Accepted 26 July 2021

Available online 1 September 2021

Editor: C.M. Petrone

#### Keywords:

basaltic magma  
magma degassing  
percolation threshold  
vesicle size distribution  
polydispersivity  
eruptive style

### ABSTRACT

Due to their generally low eruptive melt viscosities and concomitant high diffusivities of volatiles, basaltic magmas degas relatively efficiently. This relative efficiency, combined with variations in style, extent, timing and length scales of degassing govern the range of eruptive styles observed at basaltic volcanoes. The result is a surprising complexity of degassing regimes and products in basaltic volcanism. In particular, the transition between closed- and open-system degassing at low pressure at the percolation threshold may strongly affect the type of eruption. Here we aim to better understand degassing and gas percolation processes in basaltic magmas and their implications for eruptive style. Combining new and literature data, we present a database of vesicle metrics in basaltic rocks including vesicularity, vesicle number density, vesicle size distribution (and its polydispersivity), vesicle connectivity and permeability. We combine these textural and petrophysical data with a numerical model of percolation for systems having polydisperse vesicle size distributions. Using this model, we also evaluate different definitions of vesicle connectivity inherent to different measurement techniques. Our results show that polydispersivity exerts a strong control on the percolation threshold of basaltic magmas and consequently on eruptive style. Intermediate to highly polydisperse bubble networks are more typical of Hawaiian activity and are characterized by higher values of percolation threshold. This results in delayed coalescence and an increase in magma vesicularity hindering the formation of large decoupled and buoyant bubbles, which in turn can promote magma acceleration, fragmentation by inertia below the percolation threshold and sustained fountaining activity. Bubble populations with lower polydispersivity, typical of Strombolian eruptions, promote early coalescence prior to fragmentation, which in turn may lead to the formation of large decoupled slugs or gas pockets and/or plugs at the surface via outgassing. Further, we discuss the implications of our findings for Plinian, violent Strombolian, Surtseyan, deep submarine and effusive basaltic eruptions.

© 2021 The Author(s). Published by Elsevier B.V. This is an open access article under the CC BY-NC-ND license (<http://creativecommons.org/licenses/by-nc-nd/4.0/>).

### 1. Introduction

Basaltic volcanic eruptions are highly diverse in term of eruptive styles and intensities, ranging from effusive to mild explosive Hawaiian fountaining and Strombolian eruptions, to high intensity explosive eruptions such as Vulcanian, Subplinian and even Plinian.

In addition, basaltic eruptions can occur in both subaerial and subaqueous settings which influences further eruptive phenomena. Interdependent conduit processes and complex feedbacks between magma properties such as ascent rate, viscosity, crystallinity, magma-water interaction, ease of gas escape and fragmentation mechanism control the style of basaltic eruptions and especially the transition between explosive and effusive activity (e.g., Giordano and Dingwell, 2003; Namiki and Manga, 2008; Moitra et al., 2018; La Spina et al., 2021). All these processes and properties are strongly influenced by the conditions of pre- and syn-eruptive magma degassing.

\* Corresponding author at: Department für Geo- und Umweltwissenschaften, Sektion Mineralogie, Petrologie und Geochemie, Theresienstr. 41, 80333 München, Germany.

E-mail address: [mathieu.colombier@min.uni-muenchen.de](mailto:mathieu.colombier@min.uni-muenchen.de) (M. Colombier).

The formation of a gaseous phase (dominantly H<sub>2</sub>O and CO<sub>2</sub>) plays an important role in forcing magma to Earth's surface and generating basaltic eruptions. Degassing proceeds by volatile exsolution and subsequent vesiculation via bubble nucleation, growth and coalescence, potentially continuing until bubble collapse and/or migration and gas escape from the magma (Toramaru, 1989). The kinetics of degassing influence vesicle characteristics preserved in basaltic rocks such as vesicularity/porosity, vesicle size distribution (VSD) and polydispersivity, vesicle number density, vesicle connectivity and permeability.

As noted at the outset, degassing in basaltic magmas contrasts strongly with degassing in intermediate to silicic magmas mostly as a result of the lower melt viscosity (Gonnermann and Manga, 2007) and the corresponding higher diffusivity of volatiles in basaltic melts (Sparks, 1978; Dingwell, 1995). Gardner et al. (1996) propose that the rate of vesiculation is inversely proportional to magma viscosity. The low viscosity of crystal-poor basaltic magmas increases the ease of coalescence (Nguyen et al., 2013; Gonnermann and Manga, 2007). Such rapid vesiculation and efficient coalescence in basaltic magmas can have opposing consequences for eruptive style. Although rapid vesiculation can lead to magma acceleration and inertial fragmentation (explosive scenario), efficient coalescence can cause the bubble network to transition from closed- to open-system degassing conditions favouring permeable gas escape (effusive scenario) (Namiki and Manga, 2008). Degassing in basaltic magmas during explosive eruptions starts in the reservoir and/or during magma ascent, proceeds all the way to the surface and can even continue after fragmentation during ejection of magmatic droplets. Similarly, degassing during effusive phases may continue at the surface in plugs or during transport and emplacement of lava flows (Cashman et al., 1994).

The transition from closed- to open-system degassing conditions has significant implications for the eruptive style of basaltic magmas. Closed-system degassing refers to bubble growth without system-spanning inter-bubble connectivity and therefore without an onset of permeability. On the other hand, open-system degassing (in a porous network where bubbles remain coupled to the magma) implies efficient and large-scale bubble coalescence that creates system-spanning connectivity and permeable pathways through the magma column allowing gas to percolate and escape via the conduit walls or any free surface. The divide between these two end-members occurs at a critical porosity called the percolation threshold. This threshold can vary broadly in basaltic magmas depending on the polydispersivity of the VSD, crystallinity, vesicle shape and presence of cracks, and has been shown to have a first-order control on the shift between effusive and explosive eruptions (Colombier et al., 2017, 2018).

Further complications for degassing and outgassing in basaltic magmas compared to their more SiO<sub>2</sub>-rich counterparts arise from a common decoupling between the magma and the gaseous phase via the formation of buoyant meter- to conduit-sized bubbles (separated flow; Vergnolle and Jaupart, 1986). Changes in the flow regime from coupled to decoupled have been used to explain the changes between different types of mildly explosive eruptions (Vergnolle and Jaupart, 1986; Taddeucci et al., 2015). For instance, Vergnolle and Jaupart (1986) distinguish (i) a bubbly flow regime which consists of a suspension of discrete bubbles in a continuous liquid, (ii) a slug or intermittent regime in which coalescence forms cyclically large bubbles occupying the conduit diameter or (iii) an annular flow regime in which coalescence forms a continuous gas jet in the centre of the conduit. Linking these regimes to different volcanic settings remains, however, controversial (Gonnermann and Manga, 2013). The slug regime is often interpreted as the principal mechanism explaining typical transient Strombolian activity whereas the bubbly (Parfitt and Wilson, 1995) or annular (Vergnolle and Jaupart, 1986) flow regimes

fit better with continuous lava fountain-forming Hawaiian eruptions. More recently, Houghton et al. (2020) discuss that variations in activity for both Strombolian and Hawaiian eruption types can be explained by contrasting contributions of both large decoupled bubbles and a coupled mixture of small bubbles and basaltic melt (+/- crystals). Large meter-sized and decoupled bubbles are mostly not preserved at the scale of samples used in the laboratory for textural analysis and petrophysical measurements as they are lost at the magma free-surface via passive bursts (outgassing, no ejection of pyroclasts) or explosive bursts (with ejection of pyroclasts) (Houghton et al., 2020). An additional complication is that these different bubble populations may be formed from distinct volatile species and at different depths of the crust (Allard, 2010). In this study, we analyse the population of small bubbles that remain coupled to magma and are preserved as vesicles in pyroclasts.

Several studies used vesicle characteristics and permeability to shed light on vesiculation, closed- vs open-system degassing and gas percolation in basalts and their parental magma (e.g., Polacci et al., 2008, 2012; Kawabata et al., 2015; Colombier et al., 2017; Gurioli et al., 2018; Thivet et al., 2020a,b). In particular, pore connectivity and permeability relationships with porosity have been used to quantify the percolation threshold of basaltic magmas and to link degassing to eruptive style (e.g., Moitra, 2015; Colombier et al., 2017, 2020; Gurioli et al., 2018). Numerical simulations have also been carried out to study the relations between polydispersivity in vesicle sizes and the percolation threshold as well as the permeability (Vasseur et al., 2020). However, a comprehensive study unifying these different methods and linking vesicle characteristics to connectivity, permeability and eruptive style of basaltic magmas is still lacking.

In this study, we present such an approach in order to reconcile the results of connectivity obtained by different techniques and link these data to other textural and petrophysical properties such as vesicle size distribution and polydispersivity, vesicle number density, crystallinity and permeability. We compile literature data to create a representative database for these pore metrics to be used as input in stochastic simulations of numerical samples representative of basaltic magmas. Our compilation and simulations are combined with new He-pycnometry and gas permeameter data to bracket a full range of degassing scenarios, eruptive styles and products at basaltic volcanoes worldwide.

## 2. Methodology

### 2.1. Terminology

We use the following nomenclature for pore metrics. The term bubble is used to refer to the dynamic formation of a free gaseous phase by volatile exsolution and vesiculation in the basaltic magma. Vesicle refers to the frozen remnant of a bubble after quenching of the magma into a basaltic rock. Vesicularity is used as the vesicle content of a rock or as a synonym for bubble content when applied to a magma. The term pore includes vesicles and cracks or voids in a basaltic rock. Porosity thus corresponds to the total pore content of a basaltic rock. In this way, we use the terms bubble, vesicle or pore connectivity depending on the context. The terms vesicle and vesicularity are used to describe the porous networks of numerical simulations in which cracks are absent. We note that pore and porosity are more applicable to data obtained by He-pycnometry, whereas for X-ray computed tomography we use the terms vesicle, vesicularity and vesicle connectivity as any cracks remain mostly unresolved with this technique. Degassing is used as a general term that includes both closed-system degassing (volatile exsolution and vesiculation) and open-system degassing (outgassing), where the latter type corresponds to gas escape from the magma by (i) bubble migration (decoupling) or

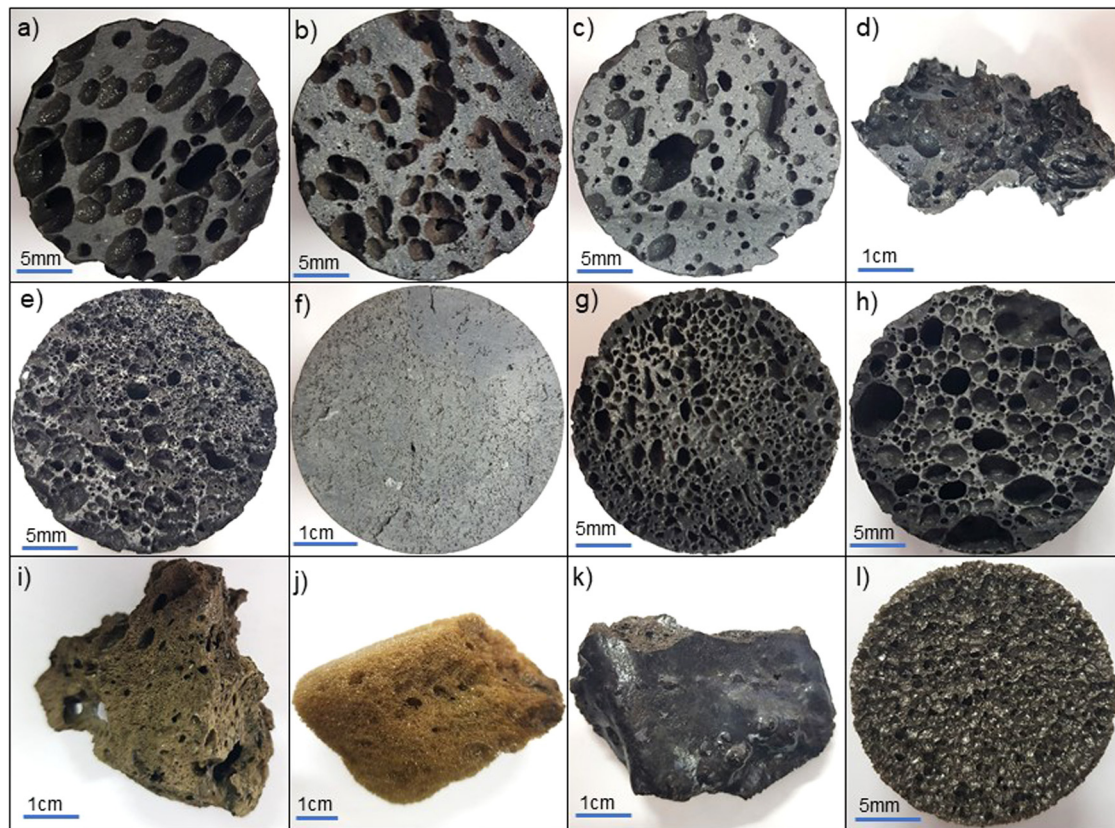


**Fig. 1.** Photos showing the textural variations in the different types of additional samples analysed in this study. a) Macrovesicular lava from the Hekla 1947 eruption, Iceland. b) Macrovesicular lava from Myvatn Fires, Iceland. c) Macrovesicular lava from Hekla 1845 eruption, Iceland. d) Macrovesicular lava from Piton de la Fournaise, La Réunion, France. e) Rim of a thin Pahoe-hoe lobe from the 1949 Llano del Banco vent of the eruption on La Palma, Canary Islands (lava sampled ~500 m from the fissure). f) Microvesicular lava from Eldgja Ayp-taver, Iceland. g and h) Bombs with different vesicle sizes from the 1973 Hawaiian lava fountaining activity at Eldfell volcano, Heimaey, Iceland. i) Pyroclast from the 3 July 2019 paroxysmal Strombolian activity at Stromboli volcano, Italy. j) Reticulite from the 1500 eruption of Kilauea volcano, Hawaii. k) Scoria with dense rim and vesicular interior from the 1959 Kilauea Iki eruption, Hawaii. l) FOAMGLAS® synthetic material used in this study.

(ii) permeable flow through an interconnected porous network (Gonnermann and Manga, 2007).

## 2.2. Measurements of porosity, connectivity and permeability

Basaltic samples from several volcanoes worldwide were collected to complete the database of porosity  $\phi$ , connectivity  $C$  and permeability  $k$ . These cover a broad range in eruptive styles, lithologies and textural features. They include scoria, Pele's tears, reticulites, golden pumices, fluidal clasts, fresh and altered pahoe-hoe and 'a'a lavas (Fig. 1).

We carried out measurements of porosity and connectivity on these new samples using a Quantachrome He-pycnometer at the Ludwig-Maximilians-Universität (LMU) in Munich, Germany. Discussion on error quantification with this technique is provided in the supplementary material.

Permeability measurements were conducted on dry, cylindrical samples at a confining pressure of 1.0 MPa in a GasPerm steady state permeameter (GPE-100, Vinci Technologies) at LMU. The gas flow across the samples was measured with a flowmeter (range 5–500 cm<sup>3</sup>.min<sup>-1</sup>) under various pressure gradients measured with a relative pressure transmitter (up to 0.69 MPa). Permeability was then obtained using Darcy's law and applying the Forchheimer or Klinkenberg corrections when necessary (see Heap et al., 2017 for a detailed procedure).

## 2.3. Data compilation

We extend the database of Colombier et al. (2017) for  $\phi$  and  $C$  obtained by He-pycnometry on basalts with measurements from

this study and with data from recent studies for basaltic rocks at different volcanoes worldwide covering a broad range of eruptive styles (Table SM1 and references therein). This increases the number of  $\phi - C$  pairs of data for basalts from  $n = 572$  in Colombier et al. (2017) to  $n = 1187$  in this study. Our present study also includes data obtained by X-ray micro-tomography for effusive and explosive basalts with different definitions of connectivity (Song et al., 2001; Polacci et al., 2008, 2012; Couves et al., 2016; Zahasky et al., 2018). Additional permeability data compared to Colombier et al. (2017) are also included (Table SM1 and references therein). Data of polydispersity in vesicle sizes  $S$ , vesicle number density  $N_V$  and crystallinity  $\phi_x$  are also compiled from literature data on basaltic rocks (Table SM2 and references therein).  $S$  values were obtained from literature data of vesicle size distributions measured by scanning electron microscopy image analysis following Vasseur et al. (2020) (Table SM2).

## 2.4. Differences between connectivity definitions

There are many different ways in which pore connectivity can be quantified. For all definitions, we use a general expression where connectivity is defined as the ratio of connected porosity to the total porosity (Colombier et al., 2017). According to variations in the measurement technique and definition of the connected pore fraction, we can further distinguish three main definitions. (i) A He-pycnometry-like definition of connectivity, hereafter referred to as  $C$ -pyc, in which all the pores connected to the exterior of a sample are counted as connected. (ii) A percolative connectivity, hereafter referred to as  $C$ -percol, for which only the pores connected from one side of the volume of interest to the opposite are

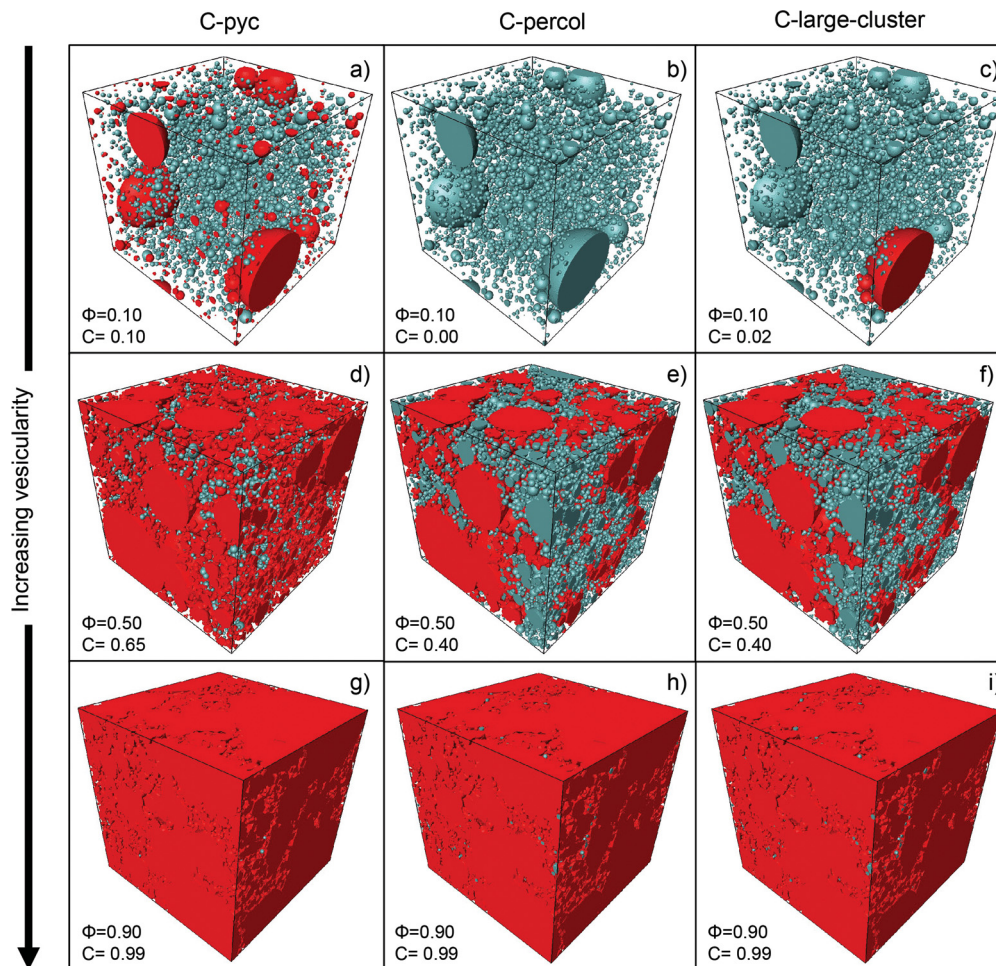


**Fig. 2.** 3D volume renderings of the simulations imaged using the software Avizo showing the discrepancies between 3D vesicle networks for the different definitions of vesicle connectivity  $C$ . A single simulation with  $S = 0.37$  was used for illustration. The red and blue-green vesicles represent the ones that are considered as connected and isolated, respectively, in each definition. Left column: pycnometry-like definition of connectivity  $C$ -pyc, for which each vesicle connected to the exterior is treated as connected. Middle column: percolative definition of connectivity  $C$ -percol, with only vesicles connected from one side to the opposite considered as connected. Right column: largest vesicle cluster definition  $C$ -large-cluster, which corresponds to the largest vesicle networks formed by local coalescence but not necessarily percolating. (For interpretation of the colours in the figure(s), the reader is referred to the web version of this article.)

considered as connected. This definition can therefore be measured in the three spatial directions of a sample and is more relevant for comparison with permeability (Colombier et al., 2017, 2018, 2020). (iii) A third definition corresponds to the largest pore cluster divided by the total porosity and is referred to as  $C$ -large-cluster. The three definitions of connectivity can be quantified using numerical simulations and X-ray computed tomography (XCT) techniques, although many authors usually quantify  $C$ -percol or  $C$ -large-cluster with XCT (e.g., Song et al., 2001; Bai et al., 2010; Polacci et al., 2008; Couves et al., 2016; Colombier et al., 2018, 2020). Fig. 2 shows 3D vesicle networks of the simulations illustrating the differences between the three definitions of connectivity at different porosities.

$C$ -pyc has the advantage that it can be measured on samples with a broad range of sizes using He-pycnometry. Helium can penetrate even into the smallest pores (Formenti and Druitt, 2003; Columbu et al., 2020) and this method therefore provides highly accurate quantification of the connected porosity. However, a major pitfall associated with this technique is that one cannot measure a connectivity of zero and that measured connectivity can be high ( $>0.5$ ) even for a non-percolating system (Fig. 2). On the other hand, connectivity data obtained using X-ray computed tomography also have important errors associated with them due to the

difficulty to resolve inter-vesicle films and cracks in highly vesicular samples (Song et al., 2001).

Here we use numerical simulation results to compare the different definitions of connectivity for vesicle networks representative of basaltic rocks and discuss the implications for measurements using He-pycnometry and for percolation processes in basaltic magmas.

## 2.5. Numerical simulations

We use a numerical framework developed in Vasseur et al. (2020) in which samples are generated by randomly placing fully overlapping spheres with polydisperse size distributions in cubic domains of different volumes. The geometric approach used in the model approximates bubbly magmas to a first order. Spheres (defined as vesicles) are randomly placed one by one in a periodic domain of a given volume until a target sphere volume fraction (defined as vesicularity) is reached. We achieve target vesicularities in the range 0.01–0.99 at 0.01 vesicularity steps. Each sphere size is drawn from a power-law distribution  $p(R)$  such that the probability that a sphere has a radius between  $R$  and  $dR$  is  $p(R) = \alpha R^{-(\alpha+1)}$ , where  $\alpha > 3$ . The shape parameter  $\alpha$  is varied across a wide range and then converted to our polydispersity metric  $S = \langle R \rangle \langle R^2 \rangle / \langle R^3 \rangle$  for which  $\langle R^n \rangle$  is the  $n$ th moment of the distribution and in the case of our power-law distribution is given by

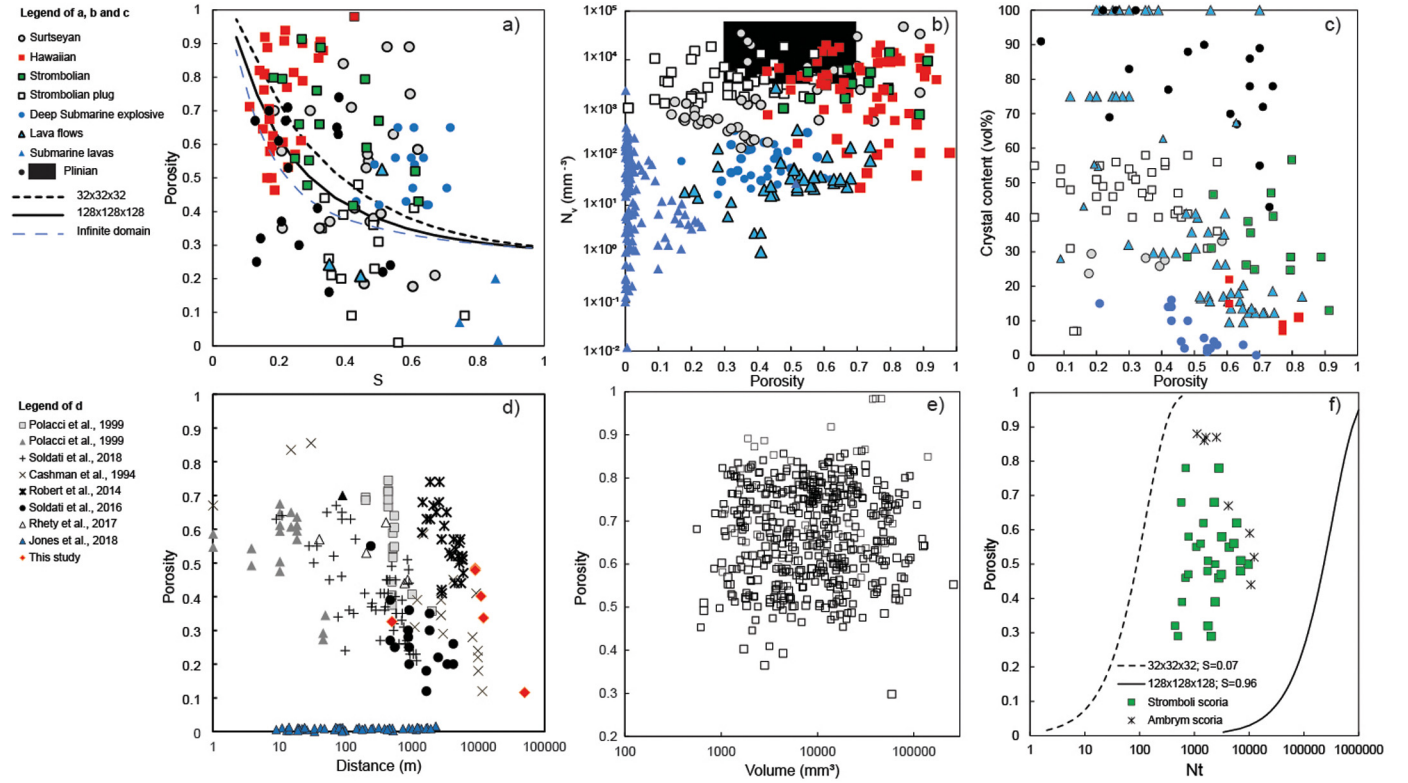


**Fig. 3.** Compilation of textural data from literature for basaltic volcanic rocks from Hawaiian, Strombolian, submarine and effusive activity. a) Porosity  $\phi$  as a function of polydispersity  $S$  ( $S = 1$  corresponds to the monodisperse limit of a vesicle size distribution). The solid and dashed curves correspond to the value of the percolation threshold  $\phi_c$  in the simulations for small, large and infinite domain sizes. b) Vesicle number density  $N_v$  (corrected for porosity and crystal content) as a function of porosity. c) Crystal content (of the melt, corrected for porosity) as a function of porosity. d) Evolution of porosity as a function of distance to the vent for different basaltic lava flows. The pattern for submarine lavas (blue triangles) with very low porosities contrasts strongly with the trend observed for subaerial lavas, with much higher values of porosity and an overall reduction of porosity with increasing distance to the vent. e) Compilation of basaltic sample volumes measured by He-pycnometry as a function of porosity. f) Comparison between the range of total number of vesicles as a function of porosity in the simulations with values from the literature for basaltic scoria analysed by X-ray computed tomography (Polacci et al., 2008, 2012).

$\langle R^n \rangle = \alpha / (\alpha - n)$  for  $n = 1, 2$  and  $3$ . We then use an adapted version of a Monte Carlo union-find algorithm (Newmann and Ziff, 2001; Vasseur et al., 2020) to check for connected sphere clusters and compute the resultant three definitions of connectivity for each generated sample. During a single simulation the vesicularity is theoretically calculated via  $\phi = 1 - \exp(-4\pi \langle R^3 \rangle N_v / 3)$  where  $N_v$  is the vesicle number density (Torquato, 2013). For each target vesicularity and given polydispersity, we run a large number of simulations anew and average the resultant values of connectivity.

Simulation features such as spherical vesicles that can freely overlap and are randomly distributed are of course simplifications of more complex systems in nature. Other numerical simulations include the effect of resistance to coalescence, vesicle shape and spatial arrangement (e.g., Blower, 2001; Giachetti et al., 2019). First, we propose that resistance to coalescence can be neglected for low viscosity basaltic melts (Blower, 2001). Second, although vesicle shape may differ from spherical for some special types of tephra such as Pele's hair, spherical vesicle networks are ubiquitous in basaltic rocks, in part due to the rather short melt relaxation times. Finally, a preferential spatial arrangement of vesicles during vesiculation in the conduit will likely have a limited effect compared to the heterogeneities observed at the scales of natural pyroclasts and induced for instance by the influence of variations in cooling rate during continued vesiculation post-fragmentation (e.g., Stovall et al., 2011).

### 3. Results

#### 3.1. Numerical simulations

To match vesicle characteristics in natural samples, we achieve a broad range of vesicularity, polydispersity, vesicle number density and volume of interest in the simulations (Figs. 3a, b and e).  $S$  for natural rocks measured using vesicle size distribution data ranges from 0.11 to 0.86 – a range that is completely covered by the simulations (0.07 to 0.96). As  $N_v$  cannot be directly compared between simulations and natural samples, we calculate the range of total number of vesicles  $N_t$  in basaltic samples of different eruptive styles, which is given by  $N_t = N_v V$  (Figs. 3b and e) where  $V$  is the sample volume and ranges mostly between  $10^3$  and  $10^5$  mm<sup>3</sup> (Fig. 3e). This calculation yields a range of  $N_t$  of  $10^4$ – $10^9$ ,  $10^5$ – $10^9$  and  $10^3$ – $10^7$  for volcanic rocks from Hawaiian, Strombolian and subaerial effusive/submarine activity measured by He pycnometry, respectively. For comparison, our simulations have  $N_t$  in the range  $10^0$ – $10^6$  and cannot be directly compared with some large samples with high number density in the database. Nonetheless, these simulations are representative of vesicle networks of a large number of basaltic lapilli and lavas from all eruptive styles studied by He-pycnometry. In addition, the range of  $N_t$  is  $10^2$ – $10^4$  for data on basaltic scoria measured by X-ray computed tomography (Polacci et al., 2008, 2012), which is completely covered by the simulations (Fig. 3f).

The different techniques and definitions used for pore connectivity have a strong influence on the relationships of connectivity with vesicularity and quantification of the percolation threshold  $\phi_c$  (Fig. 4).

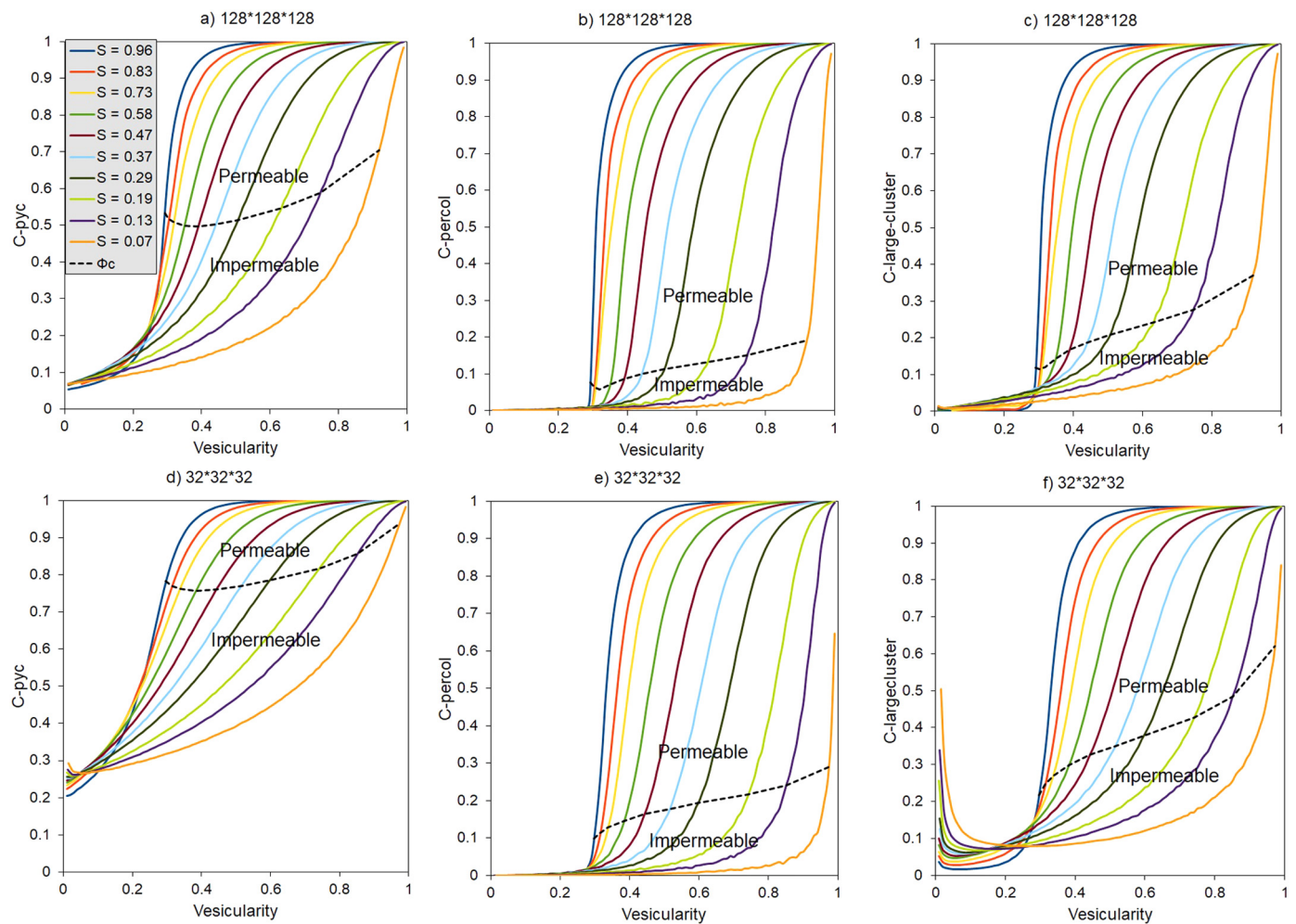


**Fig. 4.** Connectivity-vesicularity relationships obtained from the simulations for the pycnometry definition (a, d), percolation definition (b, e) and large-cluster definition (c, f), and for a range of polydispersities. a–c, Simulations performed in a large domain volume of  $128^3$ . d–f, Simulations performed in a small domain volume of  $32^3$ . The dashed line illustrates the location of the effective percolation threshold  $\phi_c$ .

With all definitions we can qualitatively grasp the increase in  $\phi_c$  caused by decreasing  $S$  from 0.96 (near-monodisperse system) to 0.07 (highly polydisperse system) (Figs. 3a and 4). That is, polydispersity raises the percolation threshold for porous networks consisting of spherical, fully overlapping objects as previously demonstrated (see Vasseur et al., 2020 for a review). The main differences are observed for the pycnometry-like definition C-pyc (Figs. 4a and d; Fig. SM5 in the supplementary material) compared to the percolating (Figs. 4b and e) and largest cluster (Figs. 4c and f) definitions. With this definition, we never obtain a connectivity of zero and connectivity can be high even for non-percolating systems (Figs. 4a and d). This discrepancy gets more pronounced as the volume of interest and subsequently the total number of vesicles decrease (Fig. 4d). For the percolating definition, we also note the presence of non-zero values of C-percol at porosities below the percolation threshold. This is a finite domain-size effect, and a percolating cluster can sometimes occur below the limiting value of  $\phi_c$  obtained independently from the percolation probability (see data repository in Vasseur et al., 2020). This method remains amongst the most reliable ones to quantify the percolation threshold. The largest cluster definition comes close to the percolating definition above  $\phi_c$  because the largest cluster generally corresponds to the percolating pathway (Figs. 4c and f), but also overestimates connectivity of non-percolating systems. Here again, the discrepancy is higher for the smaller domain size (Fig. 4f). We also note a special feature of this definition with

an initial decrease of  $C$  with  $\phi$  at low porosities (Fig. 4f). This is simply due to the fact that the largest cluster at low vesicularity generally is a single large vesicle or a few small coalesced vesicles, whose proportions decrease with the addition of isolated vesicles during the simulations.

Finally, we show the influence of the total number of vesicles on the difference between C-pyc and C-percol for the simulations and for FOAMGLAS® samples at similar value of  $S$  (Fig. 5). For the simulations, we observe similar trends for the different volumes with an initial increase of the difference as vesicles are added until the percolation threshold. The maximum difference is obtained at porosities just below the percolation threshold. After the percolation threshold is reached in the simulations, C-percol increases rapidly concomitantly with an increase in the number of vesicles and vesicularity, thereby reducing the difference between the two definitions. FOAMGLAS® samples are highly porous, non-percolating networks (C-percol=0) and therefore the discrepancy between the two definitions is expected to be high. Different volumes were analysed by pycnometry, yielding different total number of vesicles for this analogue material. We observe that the trend for FOAMGLAS® follows the trend of the simulations for the maximum difference as a function of  $N_t$ . Extrapolating this trend to higher number of vesicles allows us to estimate the value of  $N_t$  at which the difference between C-pyc and C-percol becomes zero, which yields  $N_t = 4.24 \times 10^7$  vesicles (Fig. 5).

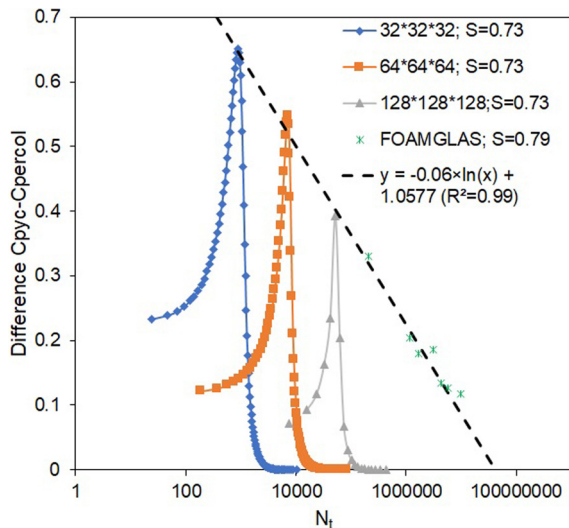


**Fig. 5.** Evolution of the difference between C-pyc and C-percol as a function of the total number of vesicles  $N_t$  used in the simulations with  $S = 0.73$ . Data for large, intermediate and small domain volumes are represented. The initial increase in the difference between the connectivity definitions corresponds to vesiculation in a non-percolating vesicle network, in which addition of vesicles leads to an increase of the fraction connected to the exterior (increase of C-pyc) but in which C-percol remains at zero. The maximum difference occurs just before the percolation threshold. At  $\phi > \phi_c$ , C-percol increases rapidly and the difference between C-pyc and C-percol therefore decreases. The difference between these two definitions is also shown for non-percolating vesicle networks in FOAMGLAS® samples of different sizes. We quantified vesicle number density of  $107 \text{ mm}^{-3}$  and a polydispersivity of  $S = 0.79$  (similar to the simulation data shown here) for this material based on analysis of XCT images (A. Ryan and J.K. Russel, pers. comm.) using FOAMS software (Shea et al., 2010). The black dashed line represents a logarithmic fitted relationship between the maximum difference and  $N_t$  for both simulations and the FOAMGLAS® material. This logarithmic trendline allowed us to estimate the minimum value of  $N_t$  required to have no more difference in connectivity data near percolation using either C-pyc and C-percol, which yields  $N_t = 4.24 \times 10^7$  vesicles for a vesicular network of similar polydispersivity.

### 3.2. Database of C vs $\phi$

Fig. 6 shows the evolution of pore connectivity C-pyc (Figs. 6a and b) and permeability (Fig. 6c) with porosity for the database of basaltic volcanic rocks compiled from the literature. Non-permeable foams including FOAMGLAS® (Ryan et al., 2019a,b; this study) and foamed rhyolitic obsidians with low  $N_t$  (Francisco Cáceres, pers. comm.) are also included for comparison.

As already discussed by Colombier et al. (2017), data for Hawaiian activity show a broader range of connectivity and extend to lower values of C-pyc than data for Strombolian eruptions. Strombolian pyroclasts exhibit two main trends that appear to be correlated to the intensity of their respective eruptions. Mild Strombolian eruptions produce pyroclasts that cluster at lower porosities than for high intensity Strombolian eruptions for a similar range of connectivity (Fig. 6). Pyroclasts from Plinian eruptions show similar porosity-connectivity ranges as those from Strombolian eruptions with high average C-pyc values.

Data for lava flows show a similar broad range of C as the pyroclasts from Hawaiian activity, but for a lower porosity window. We note that individual trends are distinct from this overall pattern, and the broad range of connectivity at low porosities is mostly observed for lavas from Pacaya volcano (Schaefer et al., 2015; Soldati et al., 2016).

Synthetic impermeable foams (FOAMGLAS®) plot at high porosity and at lower connectivity than the natural products (Fig. 6). However, decreasing the size of these synthetic samples increases connectivity from 0.12 to 0.33, which approaches the lower values measured in natural samples (Fig. 5 and 6).

The trend of permeability vs. porosity behaves similarly with a broader range of permeability for pyroclasts from Hawaiian activity than for other explosive basaltic styles, and both a reduction of average  $k$  and a scattering of data towards low porosities for lavas. It is important to note that these permeability measurements mostly include samples that have a high connectivity (with the exception of some lavas, all samples have  $C > 0.8$ ), and likely samples with a lower connectivity may plot at lower permeability or even be impermeable.

### 3.3. Comparison with simulations

Natural rocks are compared with the trends of C-pyc vs  $\phi$  from the simulations for large (Fig. 6a) and small (Fig. 6b) volumes, since  $N_t$  is unknown for most samples of the database. First, we observe that the simulated values of C-pyc vs  $\phi$  straddle 99% of the basaltic rocks from explosive activity (Figs. 6a and b). The comparison suggests that most of the C- $\phi$  trends for pyroclasts of Hawaiian and violent Strombolian activity correspond to lower average values of  $S$  (more polydisperse systems and higher  $\phi_c$ ) compared to pyroclasts from mild explosive Strombolian activity. In comparison, low porosity lavas do not fit the simulation trends.

### 3.4. Comparison with tomography data

Fig. 7 shows a comparison of C vs  $\phi$  trends obtained by XCT against those of our simulations. We also observe here that pyroclasts from Strombolian are on average better fitted by the simulated intermediate to high  $S$  trends (more monodisperse systems) and consequently low  $\phi_c$ . We note that connectivity of Strombolian pyroclasts extends to much lower values when measured with tomography as compared with He-pycnometry measurements (Figs. 6 and 7). This may be due to (i) the overestimation of pycnometry-based connectivity as discussed in this study or (ii) a lack of pixel resolution to resolve small vesicles and micro-cracks, which could lead to an underestimation of connectivity using tomography techniques. Here, we also observe that lava flows are not fitted by the simulations as in Fig. 6. Instead, the simulations of Zahasky et al. (2018) considering micro-porosity provide a better fit to the lava flow trend. Again, micro-cracks may not be resolved using XCT, affecting the measurement of the true percolating connected fraction of these lavas.

## 4. Discussion

We first focus our discussion on the comparison between the connectivity definitions obtained by different techniques and data interpretation in a volcanological context. We then discuss the role of polydispersivity on the percolation threshold and basaltic volcanic eruptions, and finally the implications for eruptive processes associated with the spectrum of basaltic eruptive styles.

### 4.1. Polydispersivity, connectivity and percolation threshold in basaltic rocks

He-pycnometry data show high connectivity for most basalts investigated here. However, a pitfall of this definition is that it treats all the pores connected to the exterior of the sample as connected. Therefore, even impermeable basaltic samples for which a percolating connectivity is zero may have an apparent connectivity higher than 0.5 with this definition. This explains the paucity of published data with C-pyc lower than 0.5 that may lead to the biased interpretation that basaltic volcanic rocks show consistently high pore connectivity. This conclusion agrees with previous studies that showed that this definition is less relevant for comparison

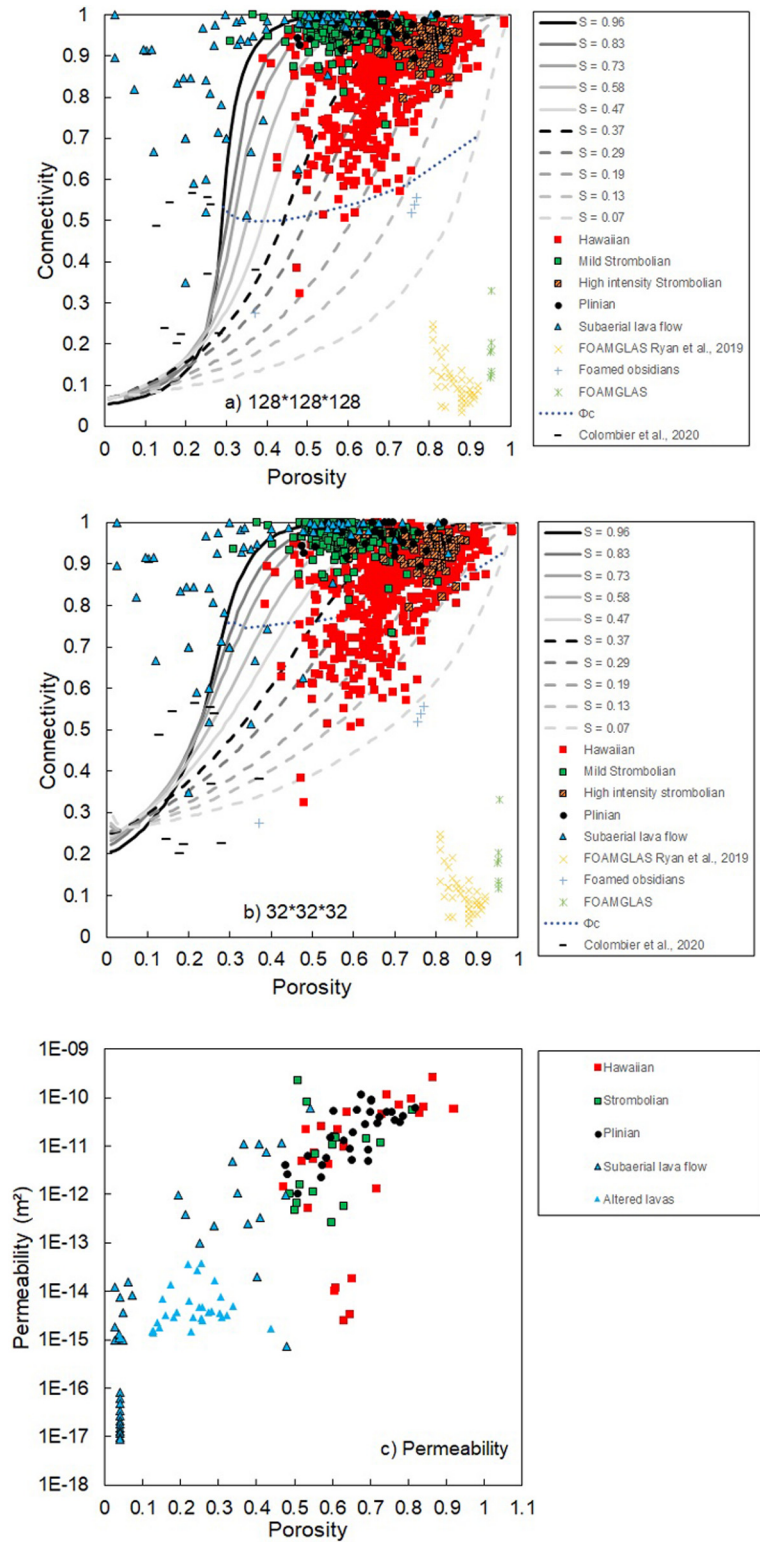


**Fig. 6.** Pycnometry-like connectivity  $C$ -pyc and permeability  $k$  as a function of porosity  $\phi$  for natural basaltic rocks and comparison with the simulations for different domain volumes and for a range of polydispersivities. This compilation includes rocks from both effusive and explosive eruptions and with a variety of eruptive styles. a)  $C$ -pyc vs  $\phi$  data from the database on basaltic products, compared with the simulations performed in a large domain volume. b)  $C$ -pyc vs  $\phi$  data compared with the simulations performed in a small domain volume. In a and b, non-permeable foamed obsidians and FOAMGLAS® samples are also shown for comparison. The dashed line corresponds to the location of the percolation threshold. In a and b, data from Colombier et al. (2020) correspond to impermeable bubble networks formed by experimental vesiculation in magma analogues with crystal contents  $\phi_x$  of 0.14-0.48. c)  $k$  vs  $\phi$  data from the database for basaltic products. Altered lavas are also included for comparison and plot at the low permeability bound of the trend.

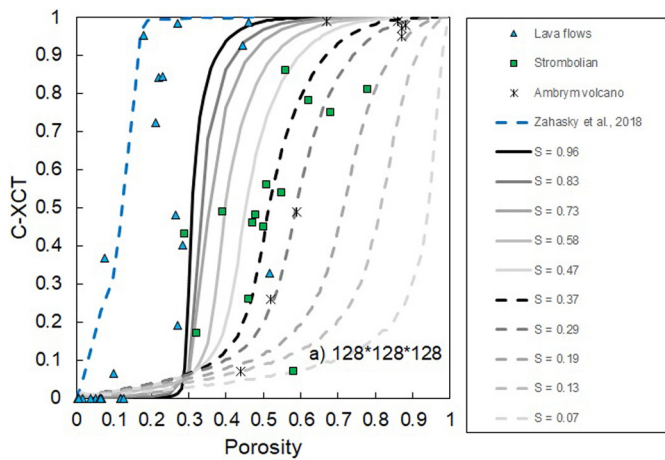


**Fig. 7.** Connectivity obtained by X-ray computed tomography (C-XCT, including both C-large cluster and C-percol definitions) as a function of  $\phi$  for data on natural basaltic rocks and comparison with different percolation models (Zahasky et al., 2018; this study). The data for explosive pyroclasts were obtained with the largest cluster definition of connectivity (Polacci et al., 2008, 2012), therefore we plot the simulation results corresponding to the same definition. For lava flows, connectivity was obtained either using the largest cluster (Song et al., 2001) or the percolation definition (Couves et al., 2016; Zahasky et al., 2018). The trend of Zahasky et al. (2018) was obtained from their Fig. 7 by dividing the effective porosity by the total porosity to derive connectivity for their 2 grid cell width microporosity median.

with permeability and quantification of  $\phi_c$  (Colombier et al., 2017, 2020).

We show that the discrepancy between the pycnometer-like definition of connectivity and definitions which are closer to a percolation model (C-percol and C-large-cluster) increases when the total number of vesicles  $N_t$  in the sample decreases (either for low  $N_V$  samples, small analysed volumes or a combination of both). For  $N_t > 4.24 \times 10^7$ , we expect little difference between data using these connectivity definitions (Fig. 5). We recommend the consideration of this discrepancy when interpreting connectivity data measured by He-pycnometry.

Despite these discrepancies, trends of  $C-\phi$  obtained by He-pycnometry remain highly informative of processes happening during different types of basaltic eruptions. Regardless of the definition used, this study shows that vesicle size distribution, and in particular the polydispersivity of the VSD, has a strong influence on the percolation threshold,  $C-\phi$  relationships and consequently on the eruptive style of basaltic magmas. Lower values of  $S$  (more polydisperse systems) lead to higher values of  $\phi_c$  (Fig. 3a). This may result in a later onset or absence of system-spanning coalescence, and a delayed onset of connectivity and open-system degassing (outgassing) prior to basaltic eruptions. On the other hand, high values of  $S$  promote lower  $\phi_c$ , and may also promote outgassing in the conduit. We discuss in the next sections how this observation can be interpreted to explain the difference between Hawaiian and Strombolian eruptions.

The  $C-\phi$  relationships for a range of  $S$  and  $\phi_c$  from the simulations straddle all the data envelope for explosive basaltic rocks of Strombolian, Hawaiian and Plinian activity (Fig. 6). This implies that the percolation threshold likely varies significantly for these explosive types. Although these trends suggest that the percolation threshold is strongly influenced by the polydispersivity of the VSD, we note that additional factors such as crystallinity, bubble deformation and cracking also have a strong influence on bubble coalescence and percolation (Parmigiani et al., 2017; Lindoo et al., 2017; Colombier et al., 2020). Most of the data for lava flows do not fit the simulation trends. This indicates that some additional processes are responsible for the  $C-\phi$  trends observed in these lavas (see section 4.2).

It remains important to stress that degassing during low intensity explosive activity should be considered at two distinct scales linked to the conditions of conduit flow (Houghton et al., 2020): (i) a large scale of meter-sized bubbles that are decoupled from and ascend faster than the magma, resulting in either passive bursting and outgassing at the surface without ejection of pyroclasts or explosive bursting with ejection of pyroclasts resulting in Strombolian or Hawaiian activity and (ii) a smaller scale of bubble population that corresponds to the small vesicles preserved in pyroclasts. This latter population ( $10^{-6}$ - $10^{-2}$  m) is generally coupled to the magma column and may strongly influence magma acceleration, explosive potential and eruptive style (Namiki and Manga, 2008). Next, we discuss for specific cases how our data may potentially be upscaled from the processes occurring in the small coupled population (bubbly flow) preserved and analysed in basaltic rocks to the kinetics of large decoupled bubble formation and consequences for the eruptive style of Strombolian and Hawaiian eruptions.

Although this aspect is beyond the scope of our study, we stress that the amount, nature and timing of volatile exsolution will differ strongly for different eruptive styles. In general, a more important role of  $\text{CO}_2$  is assumed for deep degassing (Allard, 2010) or for subaqueous eruptions (e.g., Schipper and White, 2010; Wallace et al., 2015), which may also have implications for bubble populations and vesicle metrics in basaltic rocks.

#### 4.2. Implication for the eruptive style of basaltic eruptions

We now discuss the link between textural and petrophysical properties of basaltic tephra and lavas, and the eruptive style of basaltic eruptions. It should be kept in mind that the eruptive styles represent end-members and that in nature a continuum may exist between these end-members.

##### 4.2.1. Hawaiian eruptive style

Different types of tephra from Hawaiian activity were analysed here, ranging from Pele's tears, fluidal scoria, golden pumice to reticulites. These clasts show the broadest variations of  $\phi$ ,  $C$ ,  $S$  and consequently  $\phi_c$  for explosive basaltic eruptions. There is a significant number of tephra from Hawaiian eruptions with low  $C$ -pyc compared to other types of basaltic eruptions. These tephra have on average lower values of  $S$  and consequently higher values of  $\phi_c$  compared to Strombolian clasts. We stress that this result holds true for two independent datasets of natural samples obtained with different methods (quantification of  $S$  based on vesicle size distribution in Fig. 3a and  $C-\phi$  trends in Fig. 6).

The high percolation threshold impedes system-spanning vesiculation in the conduit and favours the presence of small bubbles that remain coupled to the magma. This is consistent with a model of Hawaiian eruptions in which degassing is partly dominated by a bubbly flow with coupled small bubbles (Houghton et al., 2020; La Spina et al., 2021). In addition, high  $\phi_c$  values maintain high porosities without permeable gas loss in the conduit. Such high porosity in the absence of outgassing may in turn promote acceleration, inertial fragmentation and sustained lava-fountaining activity in such low viscosity basaltic magmas (Namiki and Manga, 2008).

A clear overall trend of increasing  $C$  with  $\phi$  is observed for the tephra of Hawaiian activity. This can be interpreted as a post-fragmentation vesiculation pattern in which the values of  $C$  and  $\phi$  represent different amounts of quench and vesiculation after fragmentation (Stovall et al., 2011, 2012). Rapidly quenched particles (i.e., Pele's tears), and the margins of larger pyroclasts, preserve low  $\phi$  and  $C$  representative of the state of magma at fragmentation, whereas slow cooling allows significant vesiculation and an increase of  $C$  with  $\phi$  (i.e., larger clasts or interior of transitional rim-to-core clasts; Stovall et al., 2011, 2012; Porritt et al., 2012).

In such a scenario, the state of the magma at fragmentation would correspond to  $C$ - $\phi$  values of  $\sim 0.5$  or lower, with corresponding  $\phi$  values near or below the percolation threshold. An additional process in which some dense clasts and rims are formed by post-fragmentation bubble shrinkage due to surface tension, thereby causing a densification from a high porosity foam is also plausible (Namiki et al., 2018) and may form a reversed trend of decreasing connectivity with porosity.

We postulate that the porosity at fragmentation is close to the percolation threshold during Hawaiian basaltic eruptions with rapidly quenched particles (i.e. small particles or rims) preserving textures close to this state at fragmentation. Porosity and connectivity of larger clasts further evolve by post-fragmentation vesiculation and bubble shrinkage producing the variety of clasts observed in the deposits.  $\phi_c$  may even represent the transition between effusive and explosive activity during hybrid eruptions displaying simultaneous Hawaiian fountaining (explosive;  $\phi_c$  reached after fragmentation) and lava flows (effusive;  $\phi_c$  reached before fragmentation).

#### 4.2.2. Strombolian

The  $\phi$ - $C$  trends (Figs. 6 and 7) and values of polydispersivity (Fig. 3a) suggest a lower average percolation threshold for pyroclasts of mild Strombolian activity compared to that from Hawaiian activity. We note that low porosity samples ( $\phi < 0.4$ ) that are common in the deposits of mild Strombolian activity (Fig. 3) are only represented by few datapoints in the database of connectivity. Bubble coalescence (in the context of the small, coupled bubble population) may hence occur at lower vesicularity in the conduit during mild Strombolian eruptions. This can have two different, complementary implications for eruptive style. (i) On the one hand, this promotes permeable outgassing at the top of the conduit and formation of a shallow, highly degassed, viscous plug. In addition, the lowered vesicularity limits the potential for acceleration and inertial fragmentation. (ii) On the other hand, lower values of  $\phi_c$  in the conduit may promote early and extensive bubble coalescence, possibly leading to the formation of large conduit-scale bubbles (slugs/gas pockets). A combination of plug and slug/gas pocket formation is currently widely accepted to drive most Strombolian eruptions (e.g., Oppenheimer et al., 2020). This second scenario should however be nuanced by an alternative process to form large decoupled bubbles by growth and local coalescence deep in the conduit, without necessarily the formation of a percolating porous network. In addition to the higher values of  $S$ , pyroclasts from mild Strombolian activity generally have higher crystal contents compared to Hawaiian tephra. This also promotes a reduction of the percolation threshold (e.g., Lindoo et al., 2017; Parmigiani et al., 2017; Colombier et al., 2020).

We note that Strombolian eruptions are highly variable in type and intensity, and that there may be a continuous spectrum between mild Strombolian and Hawaiian activities, as well as between high-intensity Strombolian and Vulcanian eruptions (Giordano and De Astis, 2021). Although such consideration is beyond the scope of our study, we note that high-intensity and paroxysmal activities at Stromboli volcano produce golden pumice clasts which form a distinct cluster in the  $\phi$ - $C$  plot (Fig. 6), which suggests lower average values of  $S$  and higher values of  $\phi_c$  for these eruptions compared to mild Strombolian activity. This fits with the postulation of Métrich et al. (2010) that propose that paroxysms are generated mostly by closed-system degassing (no percolation), whereas mild Strombolian activity is dominated by open-system conditions.

The  $\phi$ - $C$  plot points toward high values of connectivity for pyroclasts from Strombolian activity with the pycnometry method (Fig. 6) but not systematically with the XCT data (Fig. 7). This difference may be explained by (i) the presence of micro-cracks that

are not resolved by XCT and contribute to the total pore connectivity of these pyroclasts or (ii) the difference between the connectivity definitions used.

#### 4.2.3. Plinian eruptions

Vesicle metrics for Plinian basaltic eruptions reveal similar ranges of porosity, pore connectivity and permeability as for pyroclasts from Strombolian eruptions (Figs. 3 and 6; Moitra, 2015). The main characteristics of basaltic tephra from Plinian activity are the overall high crystallinity and high  $N_V$  values (Fig. 3; Sable et al., 2006). Violent basaltic eruptions such as sub-Plinian to Plinian are usually attributed to rheological shifts due to extensive microlite crystallization rather than differences in degassing and percolation processes. Microlite crystallization results in an increase of the magma viscosity and may promote gas overpressure and brittle fragmentation in basaltic magmas (Moitra et al., 2018; Arzilli et al., 2019; Heinrich et al., 2020). Other factors that promote basaltic Plinian eruptions are a fast decompression rate, a relatively low magma temperature and high pre-eruptive crystal content (Arzilli et al., 2019).

#### 4.2.4. Lava flows

As discussed above, basaltic lavas do not fit the vesiculation trends and likely represent more of a scattered densification trend with overall reduction of porosity with distance. Fig. 3d shows a compilation of  $\phi$  data as a function of distance for basaltic lava flows at different volcanoes worldwide (Table SM2). The key message here is that subaerial basaltic lava flows can have a similar range of porosities as for explosive basaltic ejecta close to the vent. However, despite data scatter, the range of porosities shows an overall decrease with increasing distance from the vent. We also observe a scattered decrease and broadening in connectivity and permeability associated with this decrease in porosity (Fig. 6). Reduction of porosity, connectivity and permeability with distance may be caused by outgassing and pore collapse, as well as by Ostwald ripening. A reverse trend may occur locally during slow emplacement and cooling potentially leading to bubble expansion and coalescence causing an increase of vesicularity in time in the lava flows (Cashman et al., 1994). On the other hand, the formation of micro-cracks may increase pore connectivity by connecting isolated bubbles. We note that additional nucleation and growth of isolated bubbles would increase the porosity but decrease connectivity, causing further scattering in the data.  $C$ - $\phi$  trends dominated by micro-porosity are consistent with the model of Zahasky et al. (2018), which describes the evolution of  $C$  with  $\phi$  in the presence of micro-porosity (Fig. 7).

#### 4.2.5. Submarine activity

The absence of connectivity data for basaltic submarine lavas and tephra impedes significant interpretation for the role of polydispersivity on the percolation threshold for these eruptive activities. However, we can use the  $N_V$  and  $S$  data to discuss vesiculation processes and implications for the eruptive style of submarine eruptions.

First, the similar range of porosity, polydispersivity and  $N_V$  for Surtseyan and Strombolian eruptions (Fig. 3) suggests that vesiculation for these shallow to emergent subaqueous eruptions is similar as for a subaerial case pointing to a low percolation threshold, outgassing and plug/slug dynamics in the conduit. The similarities in vesicle metrics between Surtseyan and subaerial basaltic explosive eruptions further suggest that the initial fragmentation may not systematically involve interaction of magma with external water but can also be driven by vesiculation.

Deep (here defined as  $>500$  m depth) explosive basaltic eruptions are characterized by high values of  $S$  (near-monodisperse systems), a range of porosity from 0 to 0.6, low  $N_V$  values and low

crystal contents (Fig. 3). This suggests a low percolation threshold allowing the formation of large bubbles by coalescence and causing slug dynamics and deep Strombolian activity. However, some magma droplets containing small isolated vesicles may be quenched at porosities below the percolation threshold due to interaction with seawater.

Finally, deep effusive basaltic eruptions are characterized by very low porosities, high values of  $S$  and low  $N_v$  (Chavrit et al., 2012; Jones et al., 2018, 2020; Fig. 3). Such systems, therefore, likely did not reach the percolation threshold and their products mostly consist of low porosity magmas with small isolated vesicles resulting from CO<sub>2</sub> degassing (i.e., Fig. 1b in Jones et al., 2020). The limited coalescence in this case therefore impedes the formation of large bubbles, slug dynamics and explosive activity.

Although there are no data for pore connectivity of submarine basaltic eruptions, we point that microcracks formed by thermal stress due to rapid quenching when lava interacts with seawater will likely increase vesicle connectivity, even if bubble coalescence is absent or limited.

## 5. Conclusions

The broad variety in eruptive styles of basaltic volcanic eruptions is strongly influenced by the dynamics, timing and length scales of vesiculation, gas percolation or escape, and bubble collapse. Vesicle metrics of basaltic rocks reveal important information about the percolation threshold of their parental magmas and implications for eruptive style at basaltic volcanoes. The large database presented here, coupled to numerical simulations, and consideration of different connectivity definitions and their size dependence help to shed light on degassing processes in basaltic melts. We conclude that polydispersivity in bubble sizes exerts a strong control on the percolation threshold of basaltic magmas and hence may strongly influence eruptive style, effusive-explosive transitions and fragmentation processes. Future work should further explore the effects of crystals, bubble deformation, and cracking on gas percolation. Detailed studies of vesicle metrics on pyroclasts produced during closely monitored basaltic eruptions may complement the present work and help to better understand and predict transitions in eruptive style at basaltic volcanoes worldwide.

## CRedit authorship contribution statement

**Mathieu Colombier:** Conceptualization, Data curation, Formal analysis, Funding acquisition, Investigation, Methodology, Resources, Validation, Visualization, Writing – original draft, Writing – review & editing. **Jeremie Vasseur:** Data curation, Formal analysis, Investigation, Methodology, Visualization, Writing – review & editing. **Bruce F. Houghton:** Investigation, Resources, Validation, Writing – review & editing. **Francisco Cáceres:** Methodology, Resources, Writing – review & editing. **Bettina Scheu:** Methodology, Resources, Writing – review & editing. **Ulrich Kueppers:** Methodology, Resources, Writing – review & editing. **Simon Thivet:** Methodology, Resources, Writing – review & editing. **Lucia Gurioli:** Methodology, Resources, Writing – review & editing. **Cristian Montanaro:** Methodology, Resources, Writing – review & editing. **Arianna Soldati:** Methodology, Resources, Writing – review & editing. **Andrea Di Muro:** Methodology, Resources, Writing – review & editing. **Donald B. Dingwell:** Funding acquisition, Resources, Writing – review & editing.

## Declaration of competing interest

The authors declare that they have no known competing financial interests or personal relationships that could have appeared to influence the work reported in this paper.

## Acknowledgements

M.C. acknowledges funding from EUROVOLC's second Transnational Access (grant number 731070, TNA project TEPHRA) for sample collection at the Piton de la Fournaise volcano. We acknowledge the support of ERC ADG 2018 834225 (EAVESDROP), NSF EAR-1829188 as well as funding by the German Research Foundation (DFG) – Project-ID 364653263 – TRR 235. We thank the Editor Chiara Maria Petrone, as well as Giuseppe La Spina and two anonymous reviewers for their constructive comments that helped to significantly improve this paper.

## Appendix A. Supplementary material

Supplementary material related to this article can be found online at <https://doi.org/10.1016/j.epsl.2021.117134>.

## References

- Allard, P., 2010. A CO<sub>2</sub>-rich gas trigger of explosive paroxysms at Stromboli basaltic volcano, Italy. *J. Volcanol. Geotherm. Res.* 189 (3–4), 363–374. <https://doi.org/10.1016/j.jvolgeores.2009.11.018>.
- Arzilli, F., La Spina, G., Burton, M.R., Polacci, M., Le Gall, N., Hartley, M.E., et al., 2019. Magma fragmentation in highly explosive basaltic eruptions induced by rapid crystallization. *Nat. Geosci.* 12 (12), 1023–1028. <https://doi.org/10.1038/s41561-019-0468-6>.
- Bai, L., Baker, D.R., Hill, R.J., 2010. Permeability of vesicular Stromboli basaltic glass: lattice Boltzmann simulations and laboratory measurements. *J. Geophys. Res., Solid Earth* 115 (B7). <https://doi.org/10.1029/2009JB007047>.
- Blower, J., 2001. Factors controlling permeability–porosity relationships in magma. *Bull. Volcanol.* 63 (7), 497–504. <https://doi.org/10.1007/s004450100172>.
- Cashman, K.V., Mangan, M.T., Newman, S., 1994. Surface degassing and modifications to vesicle size distributions in active basalt flows. *J. Volcanol. Geotherm. Res.* 61 (1–2), 45–68. [https://doi.org/10.1016/0377-0273\(94\)00015-8](https://doi.org/10.1016/0377-0273(94)00015-8).
- Chavrit, D., Humler, E., Morizet, Y., Laporte, D., 2012. Influence of magma ascent rate on carbon dioxide degassing at oceanic ridges: message in a bubble. *Earth Planet. Sci. Lett.* 357, 376–385. <https://doi.org/10.1016/j.epsl.2012.09.042>.
- Colombier, M., Wadsworth, F.B., Gurioli, L., Scheu, B., Kueppers, U., Di Muro, A., Dingwell, D.B., 2017. The evolution of pore connectivity in volcanic rocks. *Earth Planet. Sci. Lett.* 462, 99–109. <https://doi.org/10.1016/j.epsl.2017.01.011>.
- Colombier, M., Scheu, B., Wadsworth, F.B., Cronin, S., Vasseur, J., Dobson, K.J., et al., 2018. Vesiculation and quenching during surtseyan eruptions at Hunga Tonga-Hunga Ha'apai volcano, Tonga. *J. Geophys. Res., Solid Earth* 123 (5), 3762–3779. <https://doi.org/10.1029/2017JB015357>.
- Colombier, M., Wadsworth, F.B., Scheu, B., Vasseur, J., Dobson, K.J., Cáceres, F., et al., 2020. In situ observation of the percolation threshold in multiphase magma analogues. *Bull. Volcanol.* 82 (4), 1–15. <https://doi.org/10.1007/s00445-020-1370-1>.
- Columbu, S., Mulas, M., Mundula, F., Cioni, R., 2020. Strategies for helium pycnometry density measurements of welded ignimbritic rocks. *Measurement*, 108640. <https://doi.org/10.1016/j.measurement.2020.108640>.
- Couves, C., Roberts, S., Racey, A., Troth, I., Best, A., 2016. Use of X-ray computed tomography to quantify the petrophysical properties of volcanic rocks: a case study from Tenerife, Canary Islands. *J. Pet. Geol.* 39 (1), 79–94. <https://doi.org/10.1111/jpg.12629>.
- Dingwell, D.B., 1995. Relaxation in silicate melts: some applications in petrology. In: Stebbins, J.F., Dingwell, D.B., McMillan, P.W. (Eds.), *Structure and Dynamics of Silicate Melts. In: Reviews in Mineralogy, vol. 32. Mineralogical Society of America*, pp. 21–66.
- Formenti, Y., Druitt, T.H., 2003. Vesicle connectivity in pyroclasts and implications for the fluidisation of fountain-collapse pyroclastic flows, Montserrat (West Indies). *Earth Planet. Sci. Lett.* 214 (3–4), 561–574. [https://doi.org/10.1016/S0012-821X\(03\)00386-8](https://doi.org/10.1016/S0012-821X(03)00386-8).
- Gardner, J.E., Thomas, R.M., Jaupart, C., Tait, S., 1996. Fragmentation of magma during Plinian volcanic eruptions. *Bull. Volcanol.* 58 (2–3), 144–162. <https://doi.org/10.1007/s004450050132>.
- Giachetti, T., Gonnermann, H.M., Gardner, J.E., Burgisser, A., Hajimirza, S., Earley, T.C., et al., 2019. Bubble coalescence and percolation threshold in expanding rhyolitic magma. *Geochim. Geophys. Res.* 20 (2), 1054–1074. <https://doi.org/10.1029/2018GC008006>.
- Giordano, D., Dingwell, D., 2003. Viscosity of hydrous Etna basalt: implications for Plinian-style basaltic eruptions. *Bull. Volcanol.* 65 (1), 8–14. <https://doi.org/10.1007/s00445-002-0233-2>.
- Giordano, G., De Astis, G., 2021. The summer 2019 basaltic Vulcanian eruptions (paroxysms) of Stromboli. *Bull. Volcanol.* 83 (1), 1–27. <https://doi.org/10.1007/s00445-020-01423-2>.

- Gonnermann, H.M., Manga, M., 2007. The fluid mechanics inside a volcano. *Annu. Rev. Fluid Mech.* 39, 321–356. <https://doi.org/10.1146/annurev.fluid.39.050905.110207>.
- Gonnermann, H.M., Manga, M., 2013. Dynamics of magma ascent in the volcanic conduit. In: *Modeling Volcanic Processes: The Physics and Mathematics of Volcanism*, pp. 55–84.
- Gurioli, L., Di Muro, A., Vlastélic, I., Moune, S., Thivet, S., Valer, M., et al., 2018. Integrating field, textural, and geochemical monitoring to track eruption triggers and dynamics: a case study from Piton de la Fournaise. *Solid Earth* 9 (2), 431. <https://doi.org/10.5194/se-9-431-2018>.
- Heap, M.J., Kushnir, A.R., Gilg, H.A., Wadsworth, F.B., Reuschlé, T., Baud, P., 2017. Microstructural and petrophysical properties of the Permo-Triassic sandstones (Buntsandstein) from the Soultz-sous-Forêts geothermal site (France). *Geotherm. Energy* 5 (1), 26. <https://doi.org/10.1186/s40517-017-0085-9>.
- Heinrich, M., Cronin, S.J., Torres-Orozco, R., Colombier, M., Scheu, B., Pardo, N., 2020. Micro-porous pyroclasts reflecting multi-vent basaltic-andesite Plinian eruptions at Mt. Tongariro, New Zealand. *J. Volcanol. Geotherm. Res.* 401, 106936. <https://doi.org/10.1016/j.jvolgeores.2020.106936>.
- Houghton, B.F., Tisdale, C.M., Llewellyn, E.W., Taddeucci, J., Orr, T.R., Walker, B.H., Patrick, M.R., 2020. The birth of a Hawaiian fissure eruption. *J. Geophys. Res., Solid Earth*, e2020JB020903. <https://doi.org/10.1029/2020JB020903>.
- Jones, M.R., Soule, S.A., Gonnermann, H.M., Le Roux, V., Clague, D.A., 2018. Magma ascent and lava flow emplacement rates during the 2011 Axial Seamount eruption based on CO<sub>2</sub> degassing. *Earth Planet. Sci. Lett.* 494, 32–41. <https://doi.org/10.1016/j.epsl.2018.04.044>.
- Jones, M.R., Soule, S.A., Liao, Y., Brodsky, H., Le Roux, V., Klein, F., 2020. Quantitative vesicle analyses and total CO<sub>2</sub> reconstruction in mid-ocean ridge basalts. *J. Volcanol. Geotherm. Res.* 407, 107109. <https://doi.org/10.1016/j.jvolgeores.2020.107109>.
- Kawabata, E., Cronin, S.J., Bebbington, M.S., Moufti, M.R.H., El-Masry, N., Wang, T., 2015. Identifying multiple eruption phases from a compound tephra blanket: an example of the AD1256 Al-Madinah eruption, Saudi Arabia. *Bull. Volcanol.* 77 (1), 6. <https://doi.org/10.1007/s00445-014-0890-y>.
- La Spina, G., Arzilli, F., Llewellyn, E.W., Burton, M.R., Clarke, A.B., Vittori, M.D.M., et al., 2021. Explosivity of basaltic lava fountains is controlled by magma rheology, ascent rate and outgassing. *Earth Planet. Sci. Lett.* 553, 116658. <https://doi.org/10.1016/j.epsl.2020.116658>.
- Lindoo, A., Larsen, J.F., Cashman, K.V., Oppenheimer, J., 2017. Crystal controls on permeability development and degassing in basaltic andesite magma. *Geology* 45 (9), 831–834. <https://doi.org/10.1130/G39157.1>.
- Métrich, N., Bertagnini, A., Di Muro, A., 2010. Conditions of magma storage, degassing and ascent at Stromboli: new insights into the volcano plumbing system with inferences on the eruptive dynamics. *J. Petrol.* 51 (3), 603–626. <https://doi.org/10.1093/petrology/egp083>.
- Moitra, P., 2015. *The rheology of particle-liquid suspensions, the shape and connectivity of vesicles in pyroclasts and implications for the Plinian eruption of basaltic magma*. Doctoral dissertation.
- Moitra, P., Gonnermann, H.M., Houghton, B.F., Tiwary, C.S., 2018. Fragmentation and Plinian eruption of crystallizing basaltic magma. *Earth Planet. Sci. Lett.* 500, 97–104. <https://doi.org/10.1016/j.epsl.2018.08.003>.
- Namiki, A., Manga, M., 2008. Transition between fragmentation and permeable outgassing of low viscosity magmas. *J. Volcanol. Geotherm. Res.* 169 (1–2), 48–60. <https://doi.org/10.1016/j.jvolgeores.2007.07.020>.
- Namiki, A., Tanaka, Y., Yokoyama, T., 2018. Physical characteristics of scoriae and ash from 2014–2015 eruption of Aso Volcano, Japan. *Earth Planets Space* 70 (1), 1–21. <https://doi.org/10.1186/s40623-018-0914-5>.
- Newmann, M.E.J., Ziff, R.M., 2001. Fast Monte Carlo algorithm for site or bond percolation. *Phys. Rev. E* 64, 016706. <https://doi.org/10.1103/PhysRevE.64.016706>.
- Nguyen, C.T., Gonnermann, H.M., Chen, Y., Huber, C., Maiorano, A.A., Gouldstone, A., Dufek, J., 2013. Film drainage and the lifetime of bubbles. *Geochim. Geophys. Res.* 14 (9), 3616–3631. <https://doi.org/10.1002/ggge.20198>.
- Oppenheimer, J., Capponi, A., Cashman, K.V., Lane, S.J., Rust, A.C., James, M.R., 2020. Analogue experiments on the rise of large bubbles through a solids-rich suspension: a “weak plug” model for Strombolian eruptions. *Earth Planet. Sci. Lett.* 531, 115931. <https://doi.org/10.1016/j.epsl.2019.115931>.
- Parfitt, E.A., Wilson, L., 1995. Explosive volcanic eruptions - IX. The transition between Hawaiian-style lava fountaining and Strombolian explosive activity. *Geophys. J. Int.* 121, 226–232. <https://doi.org/10.1111/j.1365-246X.1995.tb03523.x>.
- Parmigiani, A., Degruyter, W., Leclaire, S., Huber, C., Bachmann, O., 2017. The mechanics of shallow magma reservoir outgassing. *Geochim. Geophys. Res.* 18 (8), 2887–2905. <https://doi.org/10.1002/2017GC006912>.
- Polacci, M., Baker, D.R., Bai, L., Mancini, L., 2008. Large vesicles record pathways of degassing at basaltic volcanoes. *Bull. Volcanol.* 70 (9), 1023–1029. <https://doi.org/10.1007/s00445-007-0184-8>.
- Polacci, M., Baker, D.R., La Rue, A., Mancini, L., Allard, P., 2012. Degassing behaviour of vesiculated basaltic magmas: an example from Ambrym volcano, Vanuatu Arc. *J. Volcanol. Geotherm. Res.* 233, 55–64. <https://doi.org/10.1016/j.jvolgeores.2012.04.019>.
- Porritt, L.A., Russell, J.K., Quane, S.L., 2012. Pele's tears and spheres: examples from Kilauea Iki. *Earth Planet. Sci. Lett.* 333, 171–180. <https://doi.org/10.1016/j.epsl.2012.03.031>.
- Ryan, A.G., Russell, J.K., Heap, M.J., Kolzenburg, S., Vona, A., Kushnir, A.R.L., 2019a. Strain-dependent rheology of silicate melt foams: importance for outgassing of silicic lavas. *J. Geophys. Res., Solid Earth* 124 (8), 8167–8186. <https://doi.org/10.1029/2019JB018099>.
- Ryan, A.G., Kolzenburg, S., Vona, A., Heap, M.J., Russell, J.K., Badger, S., 2019b. A proxy for magmatic foams: FOAMGLAS<sup>®</sup>, a closed-cell glass insulation. *J. Non-Cryst. Solids* 1, 100001. <https://doi.org/10.1016/j.nocx.2018.100001>.
- Sable, J.E., Houghton, B.F., Del Carlo, P., Coltelli, M., 2006. Changing conditions of magma ascent and fragmentation during the Etna 122 BC basaltic Plinian eruption: evidence from clast microtextures. *J. Volcanol. Geotherm. Res.* 158 (3–4), 333–354. <https://doi.org/10.1016/j.jvolgeores.2006.07.006>.
- Schaefer, L.N., Kendrick, J.E., Oommen, T., Lavallée, Y., Chigna, G., 2015. Geomechanical rock properties of a basaltic volcano. *Front. Earth Sci.* 3, 29. <https://doi.org/10.3389/feart.2015.00029>.
- Schipper, C.L., White, J.D., 2010. No depth limit to hydrovolcanic limu o Pele: analysis of limu from Lōihi Seamount, Hawaii. *Bull. Volcanol.* 72 (2), 149–164. <https://doi.org/10.1007/s00445-009-0315-5>.
- Shea, T., Houghton, B.F., Gurioli, L., Cashman, K.V., Hammer, J.E., Hobden, B.J., 2010. Textural studies of vesicles in volcanic rocks: an integrated methodology. *J. Volcanol. Geotherm. Res.* 190 (3–4), 271–289. <https://doi.org/10.1016/j.jvolgeores.2009.12.003>.
- Soldati, A., Sehlke, A., Chigna, G., Whittington, A., 2016. Field and experimental constraints on the rheology of arc basaltic lavas: the January 2014 eruption of Pacaya (Guatemala). *Bull. Volcanol.* 78 (6), 43. <https://doi.org/10.1007/s00445-016-1031-6>.
- Song, S.R., Jones, K.W., Lindquist, B.W., Dowd, B.A., Sahagian, D.L., 2001. Synchrotron X-ray computed microtomography: studies on vesiculated basaltic rocks. *Bull. Volcanol.* 63 (4), 252–263. <https://doi.org/10.1007/s004450100141>.
- Sparks, R.S.J., 1978. The dynamics of bubble formation and growth in magmas: a review and analysis. *J. Volcanol. Geotherm. Res.* 3 (1–2), 1–37. [https://doi.org/10.1016/0377-0273\(78\)90002-1](https://doi.org/10.1016/0377-0273(78)90002-1).
- Stovall, W.K., Houghton, B.F., Gonnermann, H., Fagents, S.A., Swanson, D.A., 2011. Eruption dynamics of Hawaiian-style fountains: the case study of episode 1 of the Kilauea Iki 1959 eruption. *Bull. Volcanol.* 73 (5), 511–529. <https://doi.org/10.1007/s00445-010-0426-z>.
- Stovall, W.K., Houghton, B.F., Hammer, J.E., Fagents, S.A., Swanson, D.A., 2012. Vesiculation of high fountaining Hawaiian eruptions: episodes 15 and 16 of 1959 Kilauea Iki. *Bull. Volcanol.* 74 (2), 441–455. <https://doi.org/10.1007/s00445-011-0531-7>.
- Taddeucci, J., Edmonds, M., Houghton, B., James, M.R., Vergnolle, S., 2015. *Hawaiian and Strombolian eruptions*. In: *The Encyclopedia of Volcanoes*. Academic Press, pp. 485–503.
- Thivet, S., Gurioli, L., Di Muro, A., Derrien, A., Ferrazzini, V., Gouhier, M., et al., 2020a. Evidences of plug pressurization enhancing magma fragmentation during the September 2016 basaltic eruption at Piton de la Fournaise (La Réunion Island, France). *Geochim. Geophys. Res.* 21 (2), e2019GC008611. <https://doi.org/10.1029/2019GC008611>.
- Thivet, S., Gurioli, L., Di Muro, A., 2020b. Basaltic dyke eruptions at Piton de la Fournaise: characterization of the eruptive products with implications for reservoir conditions, conduit processes and eruptive dynamics. *Contrib. Mineral. Petrol.* 175 (3), 1–24. <https://doi.org/10.1007/s00410-020-1664-5>.
- Toramaru, A., 1989. Vesiculation process and bubble size distributions in ascending magmas with constant velocities. *J. Geophys. Res., Solid Earth* 94 (B12), 17523–17542. <https://doi.org/10.1029/JB094iB12p17523>.
- Torquato, S., 2013. *Random Heterogeneous Materials: Microstructure and Macroscopic Properties*. Springer Science & Business Media, New York, 703 p.
- Vasseur, J., Wadsworth, F.B., Dingwell, D.B., 2020. Permeability of polydisperse magma foam. *Geology* 48 (6), 536–540. <https://doi.org/10.1130/G47094.1>.
- Vergnolle, S., Jaupart, C., 1986. Separated two-phase flow and basaltic eruptions. *J. Geophys. Res., Solid Earth* 91 (B12), 12842–12860. <https://doi.org/10.1029/JB091iB12p12842>.
- Wallace, P.J., Plank, T., Edmonds, M., Hauri, E.H., 2015. Volatiles in magmas. In: *The Encyclopedia of Volcanoes*. Academic Press, pp. 163–183.
- Zahasky, C., Thomas, D., Matter, J., Maher, K., Benson, S.M., 2018. Multimodal imaging and stochastic percolation simulation for improved quantification of effective porosity and surface area in vesicular basalt. *Adv. Water Resour.* 121, 235–244. <https://doi.org/10.1016/j.advwatres.2018.08.009>.

## Further reading

- Gurioli, L., Harris, A.J.L., Houghton, B.F., Polacci, M., Ripepe, M., 2008. Textural and geophysical characterization of explosive basaltic activity at Villarrica volcano. *J. Geophys. Res., Solid Earth* 113 (B8). <https://doi.org/10.1029/2007JB005328>.
- Gurioli, L., Colo, L., Bollasina, A.J., Harris, A.J., Whittington, A., Ripepe, M., 2014. Dynamics of Strombolian explosions: inferences from field and laboratory studies of erupted bombs from Stromboli volcano. *J. Geophys. Res., Solid Earth* 119 (1), 319–345. <https://doi.org/10.1002/2013JB010355>.
- Heap, M.J., Reuschlé, T., Farquharson, J.L., Baud, P., 2018. Permeability of volcanic rocks to gas and water. *J. Volcanol. Geotherm. Res.* 354, 29–38. <https://doi.org/10.1016/j.jvolgeores.2018.02.002>.

- Jones, M.R., 2019. Geophysical and geochemical constraints on submarine volcanic processes. Doctoral dissertation, Massachusetts Institute of Technology.
- Lautze, N.C., Houghton, B.F., 2007. Linking variable explosion style and magma textures during 2002 at Stromboli volcano, Italy. *Bull. Volcanol.* 69 (4), 445–460. <https://doi.org/10.1007/s00445-006-0086-1>.
- Mattsson, H.B., 2010. Textural variation in juvenile pyroclasts from an emergent, Surtseyan-type, volcanic eruption: the Capelas tuff cone, São Miguel (Azores). *J. Volcanol. Geotherm. Res.* 189 (1–2), 81–91. <https://doi.org/10.1016/j.jvolgeores.2009.10.007>.
- Mueller, S. Permeability and porosity as constraints on the explosive eruption of magma: laboratory experiments and field investigations. Doctoral dissertation, LMU.
- Murtagh, R.M., White, J.D., 2013. Pyroclast characteristics of a subaqueous to emergent Surtseyan eruption, Black Point volcano, California. *J. Volcanol. Geotherm. Res.* 267, 75–91. <https://doi.org/10.1016/j.jvolgeores.2013.08.015>.
- Parcheta, C.E., Houghton, B.F., Swanson, D.A., 2013. Contrasting patterns of vesiculation in low, intermediate, and high Hawaiian fountains: a case study of the 1969 Mauna Ulu eruption. *J. Volcanol. Geotherm. Res.* 255, 79–89. <https://doi.org/10.1016/j.jvolgeores.2013.01.016>.
- Polacci, M., Cashman, K.V., Kauahikaua, J.P., 1999. Textural characterization of the pāhoehoe–‘a‘a transition in Hawaiian basalt. *Bull. Volcanol.* 60 (8), 595–609. <https://doi.org/10.1007/s004450050254>.
- Rhétý, M., Harris, A., Villeneuve, N., Gurioli, L., Médard, E., Chevrel, O., Bachelery, P., 2017. A comparison of cooling-limited and volume-limited flow systems: examples from channels in the Piton de la Fournaise April 2007 lava-flow field. *Geochem. Geophys. Geosyst.* 18 (9), 3270–3291. <https://doi.org/10.1002/2017GC006839>.
- Robert, B., Harris, A., Gurioli, L., Médard, E., Sehlke, A., Whittington, A., 2014. Textural and rheological evolution of basalt flowing down a lava channel. *Bull. Volcanol.* 76 (6), 824. <https://doi.org/10.1007/s00445-014-0824-8>.
- Rust, A.C., Russell, J.K., Knight, R.J., 1999. Dielectric constant as a predictor of porosity in dry volcanic rocks. *J. Volcanol. Geotherm. Res.* 91 (1), 79–96. [https://doi.org/10.1016/S0377-0273\(99\)00055-4](https://doi.org/10.1016/S0377-0273(99)00055-4).
- Schipper, C.I., White, J.D., Houghton, B.F., 2010. Syn- and post-fragmentation textures in submarine pyroclasts from Lōihi Seamount, Hawaii. *J. Volcanol. Geotherm. Res.* 191 (1–2), 93–106. <https://doi.org/10.1016/j.jvolgeores.2010.01.002>.
- Verolino, A., White, J.D.L., Dürig, T., Cappuccio, F., 2019. Black Point–Pyroclasts of a Surtseyan eruption show no change during edifice growth to the surface from 100 m water depth. *J. Volcanol. Geotherm. Res.* 384, 85–102. <https://doi.org/10.1016/j.jvolgeores.2019.07.013>.